Featured in Physics

Polarization-Dependent Forces and Torques at Resonance in a Microfiber-Microcavity System

Jinsheng Lu,[1] Vincent Ginis,[1,2,*] Cheng-Wei Qiu,[3] and Federico Capasso[1,†]
[1]Harvard John A. Paulson School of Engineering and Applied Sciences, 9 Oxford Street, Cambridge, Massachusetts 02138, USA
[2]Data Lab and Applied Physics, Vrije Universiteit Brussel, 1050 Brussel, Belgium
[3]Department of Electrical and Computer Engineering, National University of Singapore, Singapore 117583, Singapore

(Received 12 December 2022; accepted 20 March 2023; published 1 May 2023)

Spin-orbit interactions in evanescent fields have recently attracted significant interest. In particular, the transfer of the Belinfante spin momentum perpendicular to the propagation direction generates polarization-dependent lateral forces on particles. However, it is still elusive as to how the polarization-dependent resonances of large particles synergize with the incident light's helicity and resultant lateral forces. Here, we investigate these polarization-dependent phenomena in a microfiber-microcavity system where whispering-gallery-mode resonances exist. This system allows for an intuitive understanding and unification of the polarization-dependent forces. Contrary to previous studies, the induced lateral forces at resonance are not proportional to the helicity of incident light. Instead, polarization-dependent coupling phases and resonance phases generate extra helicity contributions. We propose a generalized law for optical lateral forces and find the existence of optical lateral forces even when the helicity of incident light is zero. Our work provides new insights into these polarization-dependent phenomena and an opportunity to engineer polarization-controlled resonant optomechanical systems.

DOI: 10.1103/PhysRevLett.130.183601

The coupling between spin angular momentum (SAM) and orbital angular momentum (OAM) has attracted great interest in optics and physics in general [1–10]. The conversion from SAM to OAM of light has been made possible using anisotropic metasurfaces [3,9]. This transfer can also occur in other inhomogeneous media, including planar interfaces [11,12], and even in nonparaxial fields or paraxial fields with intensity gradients [7,10,13–19], and evanescent fields [20–26]. The interaction between light's spin and angular momentum not only reveals fundamental properties of light, but may also offer possibilities to produce new optical forces and optomechanical effects. The optical orbital rotation of particles using a strongly focused beam with circular polarization has been achieved due to the OAM converted from SAM in nonparaxial fields [13,14]. Optical lateral forces can be generated during the spin-orbit angular momentum interaction. Such forces have been widely used to sort chiral particles [27–31] and drive micromachines [32–36]. Because of the spin-Hall effect, light scatters to one side transverse to the propagation direction, depending on the helicity of incident light [1,5,6,8,37–39]. This asymmetric effect results in optical lateral forces [40,41].

In an evanescent field, a transverse spin momentum, also called the Belinfante spin momentum (BSM), can be produced by circularly polarized light because the spin density in the evanescent field is inhomogeneous [23]. The BSM is one component of the field momentum $\mathbf{P}$ defined as $\mathbf{P} = \mathrm{Re}(\mathbf{E}^* \times \mathbf{H})/2c^2 = \mathbf{P}^O + \mathbf{P}^S$, where $\mathbf{P}^O$ is the orbital momentum, proportional to the phase gradient and $\mathbf{P}^S$ is the BSM originating from the spin inhomogeneity. This BSM can exert a polarization-dependent optical lateral force on particles [42]. Note that the BSM does not exert force on a particle in the dipole approximation [43,44], but it has been shown to induce lateral forces on particles in the Mie regime [21–23].

In this Letter, we establish a comprehensive model of the BSM-induced optical lateral force in the context of a microfiber-microcavity system. Previous studies have shown that for lateral forces to occur, the incident light must have a helicity or the particle must be chiral. But this may not always be the case. Optical lateral forces induced on large particles may behave differently, e.g., significantly enhanced at the resonance condition [45–54]. For large particles at resonances, lateral forces may exist when light's helicity is zero while the particle is achiral. Besides, previous research on optical lateral forces mainly focused on the near fields on a flat surface [21–23]. In this respect, the circular geometry of optical fibers provides an exciting platform to investigate BSM-induced lateral forces and spin-orbit interactions [20]. Recently, the light-induced rotation of micro-objects and nano-objects around optical fibers has been demonstrated experimentally [55–57]. However, a comprehensive and intuitive understanding of BSMs in an evanescent field on a circular surface and their interaction with resonant particles remains elusive.

Consider a microfiber-microcavity system, as shown in Fig. 1(a). The fundamental modes guided in the microfiber are HE_{11}^{y} and HE_{11}^{z} with the polarized electric field along the y and z direction, respectively (Fig. S1 in the Supplemental Material [58]). An elliptically polarized mode $HE_{11}^{y} + e^{i\phi}HE_{11}^{z}$ can be formed by superposing the two polarization-orthogonal fundamental modes (HE_{11}^{y} and HE_{11}^{z}) with a phase difference ϕ determining the helicity $\sigma = \pm\mathrm{Im}(e^{i\phi}) = \pm\sin\phi$ ($\sigma = +\sin\phi$ for forward propagation and $\sigma = -\sin\phi$ for backward propagation) [62,63]. This mode is called the right-circularly polarized mode when $\phi = +\pi/2$ and the left-circularly polarized mode when $\phi = -\pi/2$.

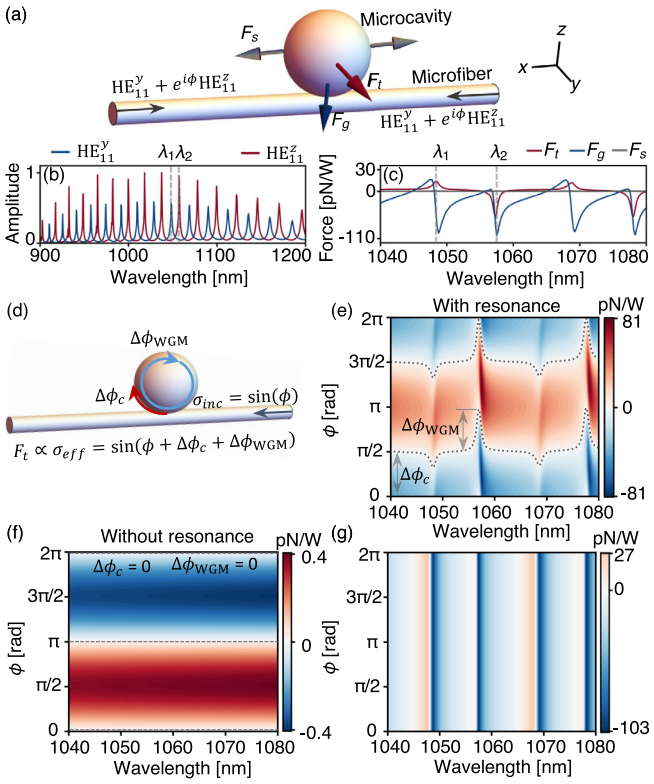

FIG. 1. A generalized law for polarization-dependent optical lateral forces at resonances. (a) Schematic of a microfiber-microcavity system. Two counterpropagating modes with the opposite helicity (forward, $\sigma = +\sin\phi$; backward, $\sigma = -\sin\phi$) are input. The radius of the microfiber r_f and the microcavity r_s is 1.33 and 5.32 μm, respectively. The refractive index of the microfiber n_{core}, the microcavity n_s, and the environment (water) n_{clad} is 1.45, 1.68, and 1.33, respectively. The gap between the fiber and the microcavity is 133 nm. (b) Electric field amplitude spectra inside the microcavity for the HE_{11}^{y} and HE_{11}^{z} modes. λ_1 (1048.6 nm) and λ_2 (1057.7 nm) are the resonance wavelength of the HE_{11}^{y} and HE_{11}^{z} modes, respectively. (c) Calculated optical lateral force F_t, gradient force F_g, and scattering force F_s on the microcavity when $\phi = \pi/2$. (d) Schematic shows two polarization-dependent phase shifts. $\Delta\phi_c$, the coupling phase shift when light couples from the fiber to the microcavity; $\Delta\phi_{\mathrm{WGM}}$, the WGM resonance phase shift. For simplicity, light incidents from the right-hand side (the principle keeps the same when light incidents from the left-hand side). (e) Calculated optical lateral force on the microcavity. (f) Calculated optical lateral force for a nanoparticle with $r_s = 250$ nm. The black dashed lines in (e) and (f) are the contour lines for $F_t = 0$ because the helicity of incident light (f) or the effective helicity after considering the phase shift effect (e) is zero on these lines. (g) Calculated gradient force on the microcavity.

To cancel out the axial scattering force and fix the microcavity's position along the microfiber direction, two counterpropagating modes are injected into the fiber. The light is coupled from the microfiber to the microcavity through the evanescent field and forms the whispering-gallery mode (WGM) inside the microcavity at the resonance wavelength. To eliminate reflections from the fiber ends, the latter can be immersed in an index-matching liquid. The spectrum of the electric field amplitude inside the microcavity is shown in Fig. 1(b). The resonance wavelengths are different for the input mode HE_{11}^{y} and HE_{11}^{z} because the effective indexes of the excited WGMs in the microcavity are not the same for different polarizations. The electric field distributions of the microfiber-microcavity system at the resonance wavelengths are shown in Fig. S9 of the Supplemental Material [58]. We use the 3D finite-difference time-domain method to simulate the electromagnetic fields of the microfiber-microcavity system. The optical forces or torques are calculated using the Maxwell stress tensor method (Sec. S1 of the Supplemental Material [58]).

We now calculate the optical forces when the forward and backward propagating modes are right- ($\sigma = 1$) and left- ($\sigma = -1$) circularly polarized, respectively. In this case, the helicity of the forward and backward propagating modes are opposite, which is to ensure that the optical lateral forces (F_t) induced by forward ($F_t \propto \sigma$) and backward ($F_t \propto -\sigma$) do not cancel out, in agreement with the previous studies [23]. As shown in Fig. 1(c), the total optical scattering force along the propagation direction (F_s) is nullified, as intended. The gradient force (F_g) between the microfiber and the microcavity is negative at most wavelengths, functioning as an attractive force between the microfiber and microcavity. However, a positive gradient force with a smaller amplitude appears at specific wavelengths, indicating a repulsive force between the microfiber and microcavity. This repulsive force in the evanescent field has also been found for metal nanoplates [64] and ring resonators [65].

Next, an optical lateral force (F_t) exists in the transverse direction of the microfiber. We provide three perspectives including the BSM (Fig. S5 [58]), the spin-to-orbital angular momentum conversion (Fig. S8 [58]), and the optical spin-Hall effect (Fig. S10 [58]) to understand the origin of this lateral force in the optical fiber system (Sec. S2 and Fig. S1 [58]). Interestingly, this optical lateral force is positive at one resonance wavelength (λ_1) and negative at the other resonance wavelength (λ_2) [Fig. 1(c)].

We also find that the asymmetric scattering from the cavity happens at these two resonance wavelengths. Light scatters more to the left (right), resulting in a positive (negative) optical lateral force at the resonance wavelength λ_1 (λ_2) (Fig. S10 [58]). From this aspect, the origin of this lateral force is similar to the previously reported substrate-induced recoil force [66]. It is well known that this optical lateral force is polarization dependent. Here we find that it also depends on the wavelength. The underlying mechanism is the polarization-dependent phase shift effect due to the resonance [Fig. 1(d)], discussed in more detail in the next paragraph.

To investigate the polarization dependence of the optical forces, we change the helicity of input modes. The calculated optical lateral force of the microcavity is shown in Fig. 1(e). For comparison, the optical lateral force for a nanoparticle with a radius of 250 nm near the microfiber is also calculated, as shown in Fig. 1(f). We can find that the optical lateral force of a nanoparticle F_t is proportional to the helicity of the incident light σ_{inc}: $F_t \propto \sigma_{\mathrm{inc}} = \sin(\phi)$. The helicity of the incident light becomes zero when $\phi = 0$, π, and 2π, making the optical lateral force become zero in these situations. The optical lateral force for the microcavity is also helicity dependent. However, it does not follow the above rule as the nanoparticle. We can make this judgment by comparing the contour lines of $F_t = 0$ between the nanoparticle [Fig. 1(f)] and the microcavity [Fig. 1(e)]. It is clear that the microcavity introduces a wavelength-dependent phase shift ($\Delta\phi_{\mathrm{WGM}}$) combined with a wavelength-insensitive phase shift ($\Delta\phi_c$) compared with the nanoparticle. Note that the phase shift $\Delta\phi_c$ depends on the size of the microcavity. More specifically, at the wavelength 1040 nm, $F_t = 0$ occurs when $\phi = 0.508\pi$ or 1.508π and when $r_s = 5.32$. It shifts to 0.078π or 1.078π when $r_s = 5$ μm (Fig. S11 [58]). The origin of this wavelength-insensitive phase shift ($\Delta\phi_c$) is the polarization-dependent coupling phase from the fiber to the microcavity. The phase shift $\Delta\phi_c$ is defined as the coupling phase difference between the two polarizations ($\Delta\phi_c = \phi_{c1} - \phi_{c2}$), where ϕ_{c1} and ϕ_{c2} are the coupling phases for the two polarizations (HE_{11}^{z} and HE_{11}^{y}), respectively (see more details for $\Delta\phi_c$ in Fig. S12 [58]). The origin of the other phase shift ($\Delta\phi_{\mathrm{WGM}}$) is the polarization-dependent resonance phase of the whispering-gallery modes, happening in a narrow band. As discussed above, the resonance appears at different wavelengths for different polarizations. At the wavelength λ_1 (λ_2), a resonance exists for the HE_{11}^{y} (HE_{11}^{z}) mode but not for the HE_{11}^{z} (HE_{11}^{y}) mode, resulting in a negative (positive) phase difference $\Delta\phi_{\mathrm{WGM}} < 0$ (> 0) between the two modes, as is indicated by the downward (upward) bending of the black dashed line near the wavelength λ_1 (λ_2) in Fig. 1(e). By considering these two phase shift effects, a generalized law for the optical lateral force of the microcavity is obtained as

$$F_t \propto \sigma_{\mathrm{eff}} = \sin(\phi + \phi_s), \tag{1}$$

where σ_{eff} is the effective helicity and ϕ_s is the total phase shift ($\phi_s = \phi_c + \phi_{\mathrm{WGM}}$). This formula differs from the previous studies [$F_t \propto \sigma_{\mathrm{inc}} = \sin(\phi)$] [23,67]. The effective helicity in our formula includes the helicity of incident light and an additional helicity contribution due to the phase shift effects. This law is not limited to the microfiber-microcavity system where WGM resonances exist. This formula also works for other resonance systems (e.g., high refractive index nanoparticles, in which case the phase shift term should be modified as $\phi_s = \phi_{\mathrm{Mie}}$, which is a wavelength-dependent phase shift due to Mie-type resonances), for nonguided waves (e.g., plane waves), and for other interfaces (e.g., the surface of a metal film) (Sec. S5 and Fig. S20 [58]).

Our generalized law for the optical lateral force can explain the origin of the negative optical torque ($F_t \propto -\sigma_{\mathrm{inc}}$) in a nanofiber-Mie particle system reported recently [55]: it is a π-phase shift ($\phi_s = \pi$) due to the Mie resonance. Another interesting finding from this generalized law is that we can generate optical lateral forces even when the helicity of incident light is zero (and also, obviously, the particle is not chiral), which was previously considered impossible, as shown in Figs. 1(e) and 1(f) when $\phi = 0$ or π.

The gradient force for the microcavity is polarization independent as expected, as shown in Fig. 1(g). It is interesting to note that the optical lateral force of the microcavity is significantly enhanced and becomes comparable to the gradient force, in contrast to previous results showing that the optical lateral force of nanoparticles or Mie particles is weak and 2 orders smaller than the gradient force [21,22]. Note that a higher quality factor of the resonator does not guarantee a larger optical lateral force in this system. The relationship between the optical lateral force and the quality factor is discussed in Sec. S6 and Figs. S21–S24 [58].

To further investigate this phase shift effect, we consider the optical lateral force when varying the helicity of the forward ($\sigma_1 = \sin\phi_1$) and backward ($\sigma_2 = \sin\phi_2$) propagating modes (Fig. S13 [58]). As we discussed above, the optical lateral forces for the forward and backward propagating modes are proportional to σ and $-\sigma$, respectively. Therefore, taking the phase shift effects into consideration, the total optical lateral force is

$$F_t \propto \sigma_{1,\mathrm{eff}} - \sigma_{2,\mathrm{eff}} = \sin(\phi_1 + \phi_s) + \sin(\phi_2 + \phi_s), \tag{2}$$

where $\sigma_{1,\mathrm{eff}}$ [$= \sin(\phi_1 + \phi_s)$] and $\sigma_{2,\mathrm{eff}}$ [$= \sin(\phi_2 + \phi_s)$] is the effective helicity of the forward and backward propagating mode. The corresponding gradient force (F_g) and total optical force along the microfiber direction (F_x) are shown in Fig. S14 [58].

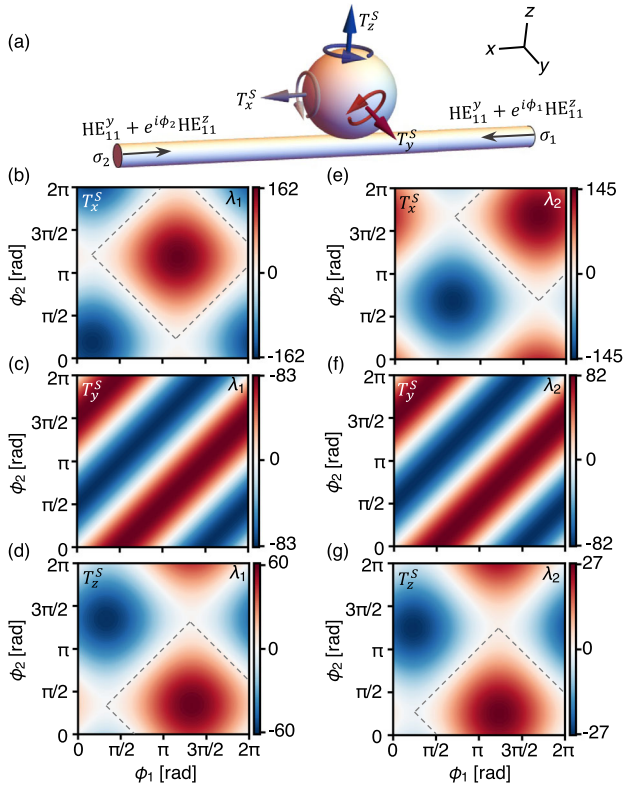

FIG. 2. Optical spin torques of the microcavity when varying the helicities of the two counterpropagating modes. (a) Schematic of the microfiber-microcavity system and the microcavity experienced optical spin torques when the two counterpropagating modes have different helicities. (b)–(g) Simulated longitudinal T_x^S (b),(e), transverse T_y^S (c),(f), and vertical T_z^S (d),(g) optical spin torques at the resonance wavelengths of $\lambda_1 = 1048.6$ nm (b)–(d) and $\lambda_2 = 1057.7$ nm (e)–(g) when varying ϕ_1 and ϕ_2. The black dashed lines forming diamond shapes in (b),(e) and (d),(g) are contour lines for $F_t = 0$, which can be predicted by Eqs. (3) and (4), respectively. The unit in (b)–(g) is pN μm/W.

We now calculate the spin torques (the light-induced torques that drive the microcavity to rotate around its own axis) when changing the helicity of forward ($\sigma_1 = \sin\phi_1$) and backward ($\sigma_2 = \sin\phi_2$) propagating modes. The simulated results are shown in Figs. 2(b)–2(g). The longitudinal spin torque T_x^S, coming from the transferring of light's SAM along the light propagating direction to the microcavity, is proportional to the effective helicity of input mode [$T_x^S \propto \sigma_{\text{eff}} = \sin(\phi + \phi_s)$], here including the phase shift effects. Therefore, the total longitudinal spin torque T_x^S for two counterpropagating modes with the same power is

$$T_x^S \propto \sigma_{1,\text{eff}} - \sigma_{2,\text{eff}} = \sin(\phi_1 + \phi_s) + \sin(\phi_2 + \phi_s). \quad (3)$$

In our analytical results, the phase shifts ϕ_s are -0.7π and -1.17π at resonance wavelengths λ_1 and λ_2, respectively (Fig. S16 [58]). The transverse spin torque T_y^S is helicity independent, however, proportional to the transverse SAM s_y (Figs. S2–S4 [58]) in the evanescent field [Figs. 2(c) and 2(f)]. Interestingly, there exists a vertical spin torque T_z^S, which is proportional to the vertical SAM s_z (Figs. S2–S4 [58]), also polarization dependent, as shown in Figs. 2(d) and 2(g). However, the vertical spin torque T_z^S behaves differently compared with the longitudinal spin torque T_x^S in two aspects. One difference is that the vertical spin torque is not helicity dependent but proportional to the degree of diagonal polarization (the normalized Stokes parameter S_2) of the input mode $\chi = \text{Re}(e^{i\phi}) = \cos\phi \in [-1, 1]$ (see Sec. S3 for the physical origin of this dependency [58]). $\chi = 1$ (-1) represents the diagonal 45 deg (−45 deg) polarization. Note that the phase shift effect should also be considered here. Therefore, the vertical spin torque is proportional to the effective degree of diagonal polarization of the input mode [$T_z^S \propto \chi_{\text{eff}} = \cos(\phi + \phi_s)$]. The other difference is that the vertical spin torque does not change direction when reversing the propagation direction of light. That is, $T_z^S \propto \chi_{\text{eff}}$ for both forward and backward propagation cases. In contrast, $T_x^S \propto \sigma_{\text{eff}}$ for the forward propagation case and $T_x^S \propto -\sigma_{\text{eff}}$ for the backward propagation case. Therefore, the total vertical spin torque T_z^S for two counterpropagating modes with the same power is related to the total effective degree of diagonal polarization by

$$T_z^S \propto \chi_{1,\text{eff}} + \chi_{2,\text{eff}} = \cos(\phi_1 + \phi_s) - \cos(\phi_2 + \phi_s), \quad (4)$$

where $\chi_{1,\text{eff}}$ [$= \cos(\phi_1 + \phi_s)$] and $\chi_{2,\text{eff}}$ [$= \cos(\phi_2 + \phi_s)$] is the effective helicity of the forward and backward propagating mode. In analytical results, the phase shifts ϕ_s are 0.67π and 0.76π at resonance wavelengths λ_1 and λ_2, respectively (Fig. S16 [58]).

By choosing two counterpropagating modes in the microfiber as the same mode $HE_{11}^y + e^{i\phi} HE_{11}^z$ [Fig. 3(a)], both the helicity σ and the degree of diagonal polarization χ of the forward ($\sigma = \sin\phi$ and $\chi = \cos\phi$) and backward ($\sigma = -\sin\phi$ and $\chi = -\cos\phi$) propagating modes are opposite. Note that $T_x^S \propto p\sigma$, $T_y^S \propto p$, and $T_z^S \propto \chi$ ($p = 1$ for forward propagation and $p = -1$ for backward propagation). In this case, the transverse spin torque T_y^S and vertical spin torque T_z^S become zero. Only the longitudinal spin torque T_x^S survives [Fig. 3(b)]. The calculated spectrum-helicity map of the longitudinal spin torque T_x^S is shown in Fig. 3(d). Note that the optical lateral (azimuthal) force and gradient force both exist in this case. By combining the attractive gradient force and the lateral force, the microcavity can orbit around the microfiber. The negative gradient force functions as a centripetal force while the optical lateral force speeds up the microcavity to obtain an orbiting velocity and eventually balances the friction force, mainly the drag force from the fluid. The calculated spectrum-helicity map of the longitudinal orbit torque T_x^O ($= \mathbf{r}_O \times \mathbf{F}_t$) is shown in Fig. 3(c); r_O is the

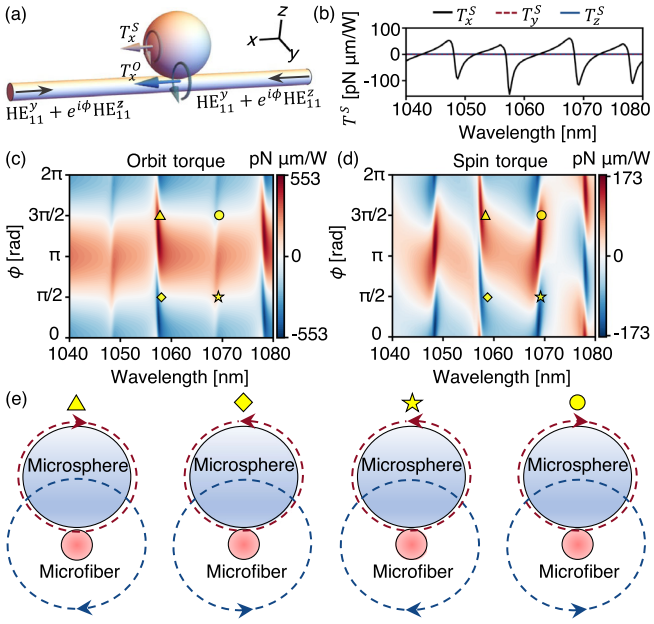

FIG. 3. Arbitrary control of optical spin torque and orbit torque in the microfiber-microcavity system. (a) Schematic of the microcavity and the longitudinal optical orbit torque and spin torque when the two counterpropagating modes have opposite helicity σ and opposite degree of diagonal polarization χ. The optical spin torques T_y^S and T_z^S are canceled out in this case. (b) Calculated optical spin torques $T_{x,y,z}^S$ of the microcavity when $\phi = \pi/2$. (c),(d) Calculated optical orbit torque T_x^O (c) and optical spin torque T_x^S (d) of the microcavity when varying ϕ. (e) Light-induced spinning and orbiting motions of the microcavity for the four selected polarizations and wavelengths (triangle, $\phi = 3\pi/2$ and $\lambda = 1058$ nm; diamond, $\phi = \pi/2$ and $\lambda = 1058$ nm; star, $\phi = \pi/2$ and $\lambda = 1069$ nm; circle, $\phi = 3\pi/2$ and $\lambda = 1069$ nm).

orbital radius of the microcavity. The 3D distribution of the longitudinal orbit-torque density inside the microcavity is shown in Fig. S17 [58]. The signs of the generated spin torques and orbit torque have all four possible combinations $(+,+)$, $(+,-)$, $(-,+)$, and $(-,-)$ whenever the incident mode is with a positive or negative spin, demonstrating the existence of both negative optical spin torques and negative optical orbit torques in this system. By selecting the suitable wavelength and helicity from the map, spinning and simultaneous orbiting multimode motions of the microcavity can be achieved, as shown in Fig. 3(e).

Note that the incident modes in the microfiber are selected as right- or left-circularly polarized modes [Figs. 3(c) and 3(d)] so that the microcavity experiences the same polarization and therefore the same torque when it moves around the microfiber, ensuring its stable and continuous rotational and orbital motions. To break this limitation, we can use radially polarized and azimuthally polarized modes in the microfiber [55,68]. According to our analysis (Sec. S4 and Fig. S19 [58]), a supporting force to the microcavity (from touching the microfiber or other repulsive forces such as the double layers forces) is required when the microcavity orbits around the microfiber in liquid environments. This is because the viscosity of the liquids is not low enough to let the microcavity quickly obtain a large orbiting velocity. It is, however, possible to achieve stable orbiting motion without the supporting force in air or vacuum.

Finally, we propose two methods to experimentally measure the optical lateral force in this microfiber-microcavity system. One method is to measure the orbiting frequency of the microcavity f_O around the microfiber driven by the optical lateral force. The optical lateral force F_t balances the drag force F_d in the liquid during the stable orbital motion [55]: $F_t = F_d = -\gamma v = -2\pi r_O f_O \gamma$, where γ is the drag coefficient. The other way is to use an optical tweezer with a trapping stiffness k to trap the microcavity near the microfiber [22]. The pump light in the microfiber causes the microcavity to move a small displacement Δy laterally away from the trapping site. The optical lateral force can then be obtained as $F_t = k\Delta y$.

In conclusion, we explored the spin-orbit interactions in a microfiber-microcavity system under resonance conditions and obtained generalized laws for describing the relationship between polarization-dependent forces or torques and the helicity of incident light. Our generalized laws are universally applicable to many resonance situations including plasmonic resonances, Mie-type resonances of dielectric nanostructures, and optical cavity resonances.

We acknowledge support from the Research Foundation Flanders under Grants No. G032822N and No. G0K9322N.

*ginis@seas.harvard.edu
†capasso@seas.harvard.edu

[1] K. Y. Bliokh, F. J. Rodríguez-Fortuño, F. Nori, and A. V. Zayats, Spin-orbit interactions of light, Nat. Photonics **9**, 796 (2015).
[2] F. Cardano and L. Marrucci, Spin-orbit photonics, Nat. Photonics **9**, 776 (2015).
[3] L. Marrucci, C. Manzo, and D. Paparo, Optical Spin-to-Orbital Angular Momentum Conversion in Inhomogeneous Anisotropic Media, Phys. Rev. Lett. **96**, 163905 (2006).
[4] O. G. Rodríguez-Herrera, D. Lara, K. Y. Bliokh, E. A. Ostrovskaya, and C. Dainty, Optical Nanoprobing via Spin-Orbit Interaction of Light, Phys. Rev. Lett. **104**, 253601 (2010).
[5] Y. Liu, Y. Ke, H. Luo, and S. Wen, Photonic spin Hall effect in metasurfaces: A brief review, Nanophotonics **6**, 51 (2017).
[6] P. Shi, A. Yang, F. Meng, J. Chen, Y. Zhang, Z. Xie, L. Du, and X. Yuan, Optical near-field measurement for spin-orbit interaction of light, Prog. Quantum Electron. **78**, 100341 (2021).

[7] S.-Y. Huang, G.-L. Zhang, Q. Wang, M. Wang, C. Tu, Y. Li, and H.-T. Wang, Spin-to-orbital angular momentum conversion via light intensity gradient, Optica **8**, 1231 (2021).

[8] X. Ling, X. Zhou, K. Huang, Y. Liu, C.-W. Qiu, H. Luo, and S. Wen, Recent advances in the spin Hall effect of light, Rep. Prog. Phys. **80**, 066401 (2017).

[9] R. C. Devlin, A. Ambrosio, N. A. Rubin, J. B. Mueller, and F. Capasso, Arbitrary spin-to–orbital angular momentum conversion of light, Science **358**, 896 (2017).

[10] P. Banzer, M. Neugebauer, A. Aiello, C. Marquardt, N. Lindlein, T. Bauer, and G. Leuchs, The photonic wheel—Demonstration of a state of light with purely transverse angular momentum, J. Eur. Opt. Soc. Rapid Publ. **8**, 13032 (2013).

[11] K. Y. Bliokh and Y. P. Bliokh, Conservation of Angular Momentum, Transverse Shift, and Spin Hall Effect in Reflection and Refraction of an Electromagnetic Wave Packet, Phys. Rev. Lett. **96**, 073903 (2006).

[12] K. Y. Bliokh, A. Niv, V. Kleiner, and E. Hasman, Geometrodynamics of spinning light, Nat. Photonics **2**, 748 (2008).

[13] Y. Zhao, J. S. Edgar, G. D. M. Jeffries, D. McGloin, and D. T. Chiu, Spin-to-Orbital Angular Momentum Conversion in a Strongly Focused Optical Beam, Phys. Rev. Lett. **99**, 073901 (2007).

[14] X.-L. Wang, J. Chen, Y. Li, J. Ding, C.-S. Guo, H.-T. Wang *et al.*, Optical Orbital Angular Momentum from the Curl of Polarization, Phys. Rev. Lett. **105**, 253602 (2010).

[15] V. Svak, O. Brzobohatý, M. Šiler, P. Jákl, J. Kaňka, P. Zemánek, and S. Simpson, Transverse spin forces and non-equilibrium particle dynamics in a circularly polarized vacuum optical trap, Nat. Commun. **9**, 1 (2018).

[16] A. Aiello, P. Banzer, M. Neugebauer, and G. Leuchs, From transverse angular momentum to photonic wheels, Nat. Photonics **9**, 789 (2015).

[17] J. Eismann, L. Nicholls, D. Roth, M. A. Alonso, P. Banzer, F. Rodríguez-Fortuño, A. Zayats, F. Nori, and K. Bliokh, Transverse spinning of unpolarized light, Nat. Photonics **15**, 156 (2021).

[18] T. A. Nieminen, A. B. Stilgoe, N. R. Heckenberg, and H. Rubinsztein-Dunlop, Angular momentum of a strongly focused Gaussian beam, J. Opt. A **10**, 115005 (2008).

[19] Y. Fang, M. Han, P. Ge, Z. Guo, X. Yu, Y. Deng, C. Wu, Q. Gong, and Y. Liu, Photoelectronic mapping of the spin-orbit interaction of intense light fields, Nat. Photonics **15**, 115 (2021).

[20] J. Petersen, J. Volz, and A. Rauschenbeutel, Chiral nanophotonic waveguide interface based on spin-orbit interaction of light, Science **346**, 67 (2014).

[21] V. Ginis, L. Liu, A. She, and F. Capasso, Using the Belinfante momentum to retrieve the polarization state of light inside waveguides, Sci. Rep. **9**, 1 (2019).

[22] L. Liu, A. Di Donato, V. Ginis, S. Kheifets, A. Amirzhan, and F. Capasso, Three-Dimensional Measurement of the Helicity-Dependent Forces on a Mie Particle, Phys. Rev. Lett. **120**, 223901 (2018).

[23] K. Y. Bliokh, A. Y. Bekshaev, and F. Nori, Extraordinary momentum and spin in evanescent waves, Nat. Commun. **5**, 3300 (2014).

[24] M. Antognozzi, C. Bermingham, R. Harniman, S. Simpson, J. Senior, R. Hayward, H. Hoerber, M. Dennis, A. Bekshaev, K. Bliokh *et al.*, Direct measurements of the extraordinary optical momentum and transverse spin-dependent force using a nano-cantilever, Nat. Phys. **12**, 731 (2016).

[25] L. Wei, A. V. Zayats, and F. J. Rodríguez-Fortuño, Interferometric Evanescent Wave Excitation of a Nanoantenna for Ultrasensitive Displacement and Phase Metrology, Phys. Rev. Lett. **121**, 193901 (2018).

[26] M. Nieto-Vesperinas and X. Xu, Reactive helicity and reactive power in nanoscale optics: Evanescent waves. Kerker conditions. Optical theorems and reactive dichroism, Phys. Rev. Res. **3**, 043080 (2021).

[27] S. Wang and C. T. Chan, Lateral optical force on chiral particles near a surface, Nat. Commun. **5**, 3307 (2014).

[28] T. Zhang, M. R. C. Mahdy, Y. Liu, J. H. Teng, C. T. Lim, Z. Wang, and C.-W. Qiu, All-optical chirality-sensitive sorting via reversible lateral forces in interference fields, ACS Nano **11**, 4292 (2017).

[29] A. Hayat, J. B. Mueller, and F. Capasso, Lateral chirality-sorting optical forces, Proc. Natl. Acad. Sci. U.S.A. **112**, 13190 (2015).

[30] L. Fang and J. Wang, Optical Trapping Separation of Chiral Nanoparticles by Subwavelength Slot Waveguides, Phys. Rev. Lett. **127**, 233902 (2021).

[31] C. Genet, Chiral light-chiral matter interactions: An optical force perspective, ACS Photonics **9**, 319 (2022).

[32] Y. Y. Tanaka, P. Albella, M. Rahmani, V. Giannini, S. A. Maier, and T. Shimura, Plasmonic linear nanomotor using lateral optical forces, Sci. Adv. **6**, eabc3726 (2020).

[33] O. Ilic and H. A. Atwater, Self-stabilizing photonic levitation and propulsion of nanostructured macroscopic objects, Nat. Photonics **13**, 289 (2019).

[34] X. Wu, R. Ehehalt, G. Razinskas, T. Feichtner, J. Qin, and B. Hecht, Light-driven microdrones, Nat. Nanotechnol. **17**, 477 (2022).

[35] D. Andrén, D. G. Baranov, S. Jones, G. Volpe, R. Verre, and M. Käll, Microscopic metavehicles powered and steered by embedded optical metasurfaces, Nat. Nanotechnol. **16**, 970 (2021).

[36] A. Canós Valero, D. Kislov, E. A. Gurvitz, H. K. Shamkhi, A. A. Pavlov, D. Redka, S. Yankin, P. Zemánek, and A. S. Shalin, Nanovortex-driven all-dielectric optical diffusion boosting and sorting concept for lab-on-a-chip platforms, Adv. Sci. **7**, 1903049 (2020).

[37] X. Yin, Z. Ye, J. Rho, Y. Wang, and X. Zhang, Photonic spin Hall effect at metasurfaces, Science **339**, 1405 (2013).

[38] D. O'connor, P. Ginzburg, F. J. Rodríguez-Fortuño, G. A. Wurtz, and A. V. Zayats, Spin-orbit coupling in surface plasmon scattering by nanostructures, Nat. Commun. **5**, 5327 (2014).

[39] M. Kim, D. Lee, Y. Kim, and J. Rho, Generalized analytic formula for spin Hall effect of light: Shift enhancement and interface independence, Nanophotonics **11**, 2803 (2022).

[40] S. Sukhov, V. Kajorndejnukul, R. R. Naraghi, and A. Dogariu, Dynamic consequences of optical spin-orbit interaction, Nat. Photonics **9**, 809 (2015).

[41] H. Magallanes and E. Brasselet, Macroscopic direct observation of optical spin-dependent lateral forces and left-handed torques, Nat. Photonics **12**, 461 (2018).

[42] K. Y. Bliokh, A. Y. Bekshaev, and F. Nori, Optical momentum and angular momentum in complex media: From the Abraham-Minkowski debate to unusual properties of surface plasmon-polaritons, New J. Phys. **19**, 123014 (2017).
[43] F. J. Belinfante, On the current and the density of the electric charge, the energy, the linear momentum and the angular momentum of arbitrary fields, Physica **7**, 449 (1940).
[44] P. C. Chaumet and M. Nieto-Vesperinas, Time-averaged total force on a dipolar sphere in an electromagnetic field, Opt. Lett. **25**, 1065 (2000).
[45] J. Ng, C. T. Chan, P. Sheng, and Z. Lin, Strong optical force induced by morphology-dependent resonances, Opt. Lett. **30**, 1956 (2005).
[46] T. Iida and H. Ishihara, Theoretical Study of the Optical Manipulation of Semiconductor Nanoparticles under an Excitonic Resonance Condition, Phys. Rev. Lett. **90**, 057403 (2003).
[47] Y. Yang, W.-P. Zang, Z.-Y. Zhao, and J.-G. Tian, Morphology-dependent resonance of the optical forces on Mie particles in an Airy beam, Opt. Express **21**, 6186 (2013).
[48] T. Zhu, Y. Shi, W. Ding, D. P. Tsai, T. Cao, A. Q. Liu, M. Nieto-Vesperinas, J. J. Sáenz, P. C. Wu, and C.-W. Qiu, Extraordinary Multipole Modes and Ultra-Enhanced Optical Lateral Force by Chirality, Phys. Rev. Lett. **125**, 043901 (2020).
[49] J. J. Xiao, J. Ng, Z. Lin, and C. T. Chan, Whispering gallery mode enhanced optical force with resonant tunneling excitation in the Kretschmann geometry, Appl. Phys. Lett. **94**, 011102 (2009).
[50] A. Einat and U. Levy, Analysis of the optical force in the micro ring resonator, Opt. Express **19**, 20405 (2011).
[51] Y. Li, O. V. Svitelskiy, A. V. Maslov, D. Carnegie, E. Rafailov, and V. N. Astratov, Giant resonant light forces in microspherical photonics, Light Sci. Appl. **2**, e64 (2013).
[52] Y. Geng, J. Tan, Y. Cao, Y. Zhao, Z. Liu, and W. Ding, Giant and tunable optical torque for micro-motors by increased force arm and resonantly enhanced force, Sci. Rep. **8**, 2819 (2018).
[53] Y. Shi, L.-M. Zhou, A. Q. Liu, M. Nieto-Vesperinas, T. Zhu, A. Hassanfiroozi, J. Liu, H. Zhang, D. P. Tsai, H. Li *et al.*, Superhybrid mode-enhanced optical torques on Mie-resonant particles, Nano Lett. **22**, 1769 (2022).
[54] A. Ashkin and J. M. Dziedzic, Observation of Resonances in the Radiation Pressure on Dielectric Spheres, Phys. Rev. Lett. **38**, 1351 (1977).
[55] G. Tkachenko, I. Toftul, C. Esporlas, A. Maimaiti, F. Le Kien, V. G. Truong, and S. N. Chormaic, Light-induced rotation of dielectric microparticles around an optical nanofiber, Optica **7**, 59 (2020).
[56] J. Lu, Q. Li, C.-W. Qiu, Y. Hong, P. Ghosh, and M. Qiu, Nanoscale Lamb wave-driven motors in nonliquid environments, Sci. Adv. **5**, eaau8271 (2019).
[57] W. Tang, W. Lyu, J. Lu, F. Liu, J. Wang, W. Yan, and M. Qiu, Micro-scale opto-thermo-mechanical actuation in the dry adhesive regime, Light Sci. Appl. **10**, 1 (2021).
[58] See Supplemental Material at http://link.aps.org/supplemental/10.1103/PhysRevLett.130.183601, which includes Refs. [59–61], for numerical simulation method, three perspectives to understand the origin of the lateral force, the transverse and vertical spin angular momentum in the microfiber, the generality of the phase shift effect law, and the relationship between optical lateral forces and the quality factor.
[59] L. Novotny and B. Hecht, *Principles of Nano-Optics* (Cambridge University Press, Cambridge, England, 2012).
[60] J. Lin, J. B. Mueller, Q. Wang, G. Yuan, N. Antoniou, X.-C. Yuan, and F. Capasso, Polarization-controlled tunable directional coupling of surface plasmon polaritons, Science **340**, 331 (2013).
[61] V. Van, *Optical Microring Resonators: Theory, Techniques, and Applications* (CRC Press, Boca Raton, 2016).
[62] F. Le Kien and A. Rauschenbeutel, Negative azimuthal force of nanofiber-guided light on a particle, Phys. Rev. A **88**, 063845 (2013).
[63] L. Fang and J. Wang, Intrinsic transverse spin angular momentum of fiber eigenmodes, Phys. Rev. A **95**, 053827 (2017).
[64] J. Lu, H. Yang, L. Zhou, Y. Yang, S. Luo, Q. Li, and M. Qiu, Light-Induced Pulling and Pushing by the Synergic Effect of Optical Force and Photophoretic Force, Phys. Rev. Lett. **118**, 043601 (2017).
[65] V. Intaraprasonk and S. Fan, A lateral optical equilibrium in waveguide-resonator optical force, Opt. Express **21**, 25257 (2013).
[66] F. J. Rodríguez-Fortuño, N. Engheta, A. Martínez, and A. V. Zayats, Lateral forces on circularly polarizable particles near a surface, Nat. Commun. **6**, 8799 (2015).
[67] Y. Shi, T. Zhu, J. Liu, D. P. Tsai, H. Zhang, S. Wang, C. T. Chan, P. C. Wu, A. V. Zayats, F. Nori *et al.*, Stable optical lateral forces from inhomogeneities of the spin angular momentum, Sci. Adv. **8**, eabn2291 (2022).
[68] Y. Zhou, X. Xu, Y. Zhang, M. Li, S. Yan, M. Nieto-Vesperinas, B. Li, C.-W. Qiu, and B. Yao, Observation of high-order imaginary Poynting momentum optomechanics in structured light, Proc. Natl. Acad. Sci. U.S.A. **119**, e2209721119 (2022).